Pupil size stability of the cubic phase mask solution for presbyopia

Citlalli Almaguer
Eva Acosta
Justo Arines

SPIE.

Pupil size stability of the cubic phase mask solution for presbyopia

Citlalli Almaguer, Eva Acosta, and Justo Arines*
Universidade de Santiago de Compostela, Facultade de Óptica e Optometría, Dept. Física Aplicada, Santiago de Compostela, Spain

Abstract. Presbyopia correction involves different types of studies such as lens design, clinical study, and the development of objective metrics, such as the visual Strehl ratio. Different contact lens designs have been proposed for presbyopia correction, but performance depends on pupil diameter. We will analyze the potential use of a nonsymmetrical element, a cubic phase mask (CPM) solution, to develop a contact or intraocular lens whose performance is nearly insensitive to changes in pupil diameter. We will show the through focus optical transfer function of the proposed element for different pupil diameters ranging from 3 to 7 mm. Additionally, we will show the images obtained through computation and experiment for a group of eye charts with different visual acuities. Our results show that a CPM shaped as 7.07 μm $* (Z_3^3 - Z_3^{-3}) - 0.9$ μm Z_2^0 is a good solution for a range of clear vision with a visual acuity of at least 0.1 logMar from 0.4 to 6 m for pupil diameters in the 3- to 7-mm range. Our results appear to be a good starting point for further development and study of this kind of CPM solution for presbyopia. © *2018 Society of Photo-Optical Instrumentation Engineers (SPIE)* [DOI: 10.1117/1.JBO.23.1.015002]

Keywords: presbyopia; pupil diameter; visual Strehl; through focus; contact lens; cubic phase; Zernike polynomials.

Paper 170342RR received May 29, 2017; accepted for publication Dec. 4, 2017; published online Jan. 2, 2018.

1 Introduction

It is well known that presbyopia is an age-dependant and progressive reduction in the amplitude of accommodation of the human eye caused by decreased flexibility of the eye lens starting around age 45.[1] The main symptom is difficulty in clearly focusing on objects up close. A number of different solutions are available to compensate for this reduction in the amplitude of accommodation that mitigates the symptoms of presbyopia, the main ones being ophthalmic lenses (monofocal, bifocal, or progressive), contact or intraocular lenses, and refractive surgery.[2–5] In this paper, we will concentrate on the ones that exploit depth of focus increased by complex wavefront, such as those proposed by Ares, Cathey, Zalevsky, Gallego, Petelczyc, Arines,[5–11] and others.

A growing number of people are turning to contact lenses to solve their presbyopia issues, mainly previous contact lens wearers who do not want to go back to glasses. There are a great many contact lens refractive profiles to increase the range of clear vision the main categories being: bifocal, multifocal, diffractive, and extended depth of focus.[2–11] Most commercial designs cover two or more regions with different refractive powers to generate more than one focus and provide good quality images of objects placed at different distances. One of the limitations of these profiles, however, is their dependence on pupil diameter.[2,4]

Preliminary evaluation of the suitability of optical solutions proposed in the literature to increase vision typically begins with numerical evaluation. Quantification of expected benefit and visual performance is based on different metrics generally grouped under the name of visual Strehl (VS) related with wavefront error, optical transfer function, point spread function, and correlation with templates.[12–18] A variety of different criteria

bear witness to the difficulty of the task. Among these, we underscore the work of Thibos et al.,[13] Iskander,[14] and Young et al.[16]

Broadly speaking, most would agree that of the different VS criteria the benchmark is the visual optical transfer function (VSOTF).[8–12] However, several authors point out that this criterion is better suited to symmetrical aberrations as opposed their high-order counterpart. In fact, they consider that when working with nonsymmetrical aberrations it is better to use metrics that emphasize the relevance of the OTF phase (PTF), especially when searching for correlations with letter identification and predicting visual acuity.[11,15–19] In a previous paper,[11] we highlighted the limitations of VSOTF in predicting the performance of a cubic phase mask (CPM) element proposed for presbyopia. We compared VSOTF and the criterion suggested by Young et al.[16] called visual Strehl combined (VS_{Combined}) with numerical simulations and experimental data. We found that for the CPM solution the VSOTF predicted the nonvisibility of the letters presenting very small values, similar to those of two-dimensional out of focus images, although they were readable. In contrast, the VS_{Combined} showed better correlation with the visual experience of the letters.[16,17]

This paper is the continuation of our previous work.[11] Here, we analyze the stability of the CPM solution of the form $A(Z_3^3 - Z_3^{-3}) - BZ_2^0$ with respect to changes in pupil diameter to assess its potential clinical applications. Z_i's represent the Zernike polynomial defined as in Ref. 19. The methodology and the VS criteria used to quantify performance are found in Sec. 2 and results in Sec. 3. Through-focus real part of the OTF and CPM performance are shown in terms of two different VS criteria, one proposed by Thibos et al., VSOTF[12,13] based on the OTF, and the other proposed by Young et al., VS_{Combined}[16] emphasizing the relative weight of the PTF on VS calculations.

---

*Address all correspondence to: Justo Arines, E-mail: justo.arines@usc.es

Several retinal images computed numerically for different eye chart distances are also provided to quantitatively demonstrate the visual performance of the CPM solution. Experimental proof of concept will also be shown. The discussion is found in section four and conclusions in Sec. 5.

2 Numerical Evaluation

To evaluate the CPM solution, we used computational Fourier optics from which we were able to compute the different VS criteria and simulate the retinal image obtained through the CPM element. The CPM consists of a phase component placed at the pupil plane of the form $[A(Z_3^3 - Z_3^{-3}) - BZ_2^0]$. Three different values of A were evaluated ($A = 0$, 3.53, and 7.07 μm] at 5-mm pupil diameter). These values were selected as an initial guess, not as a result of an optimization process. Although looking very odd they correspond to considering the CPM to have 0-, 10-, and 20-μm peak to valley at 5-mm pupil diameter. By contrast, the B value was set to 0.9 μm considering the results presented in our previous work[11] that this value provides the largest range of clear vision. The through focus real part of the modulation transfer functions, real (OTF), and retinal images were computed for four object distances corresponding to far (6 m), intermediate (1 and 0.6 m), and near vision 0.4 m, and three different pupil sizes 3.0, 5.0, and 7.0 mm, respectively. We considered a simplified model eye of 16.6-mm focal length and wavelength 578 nm. We included the Stiles–Crawford effect (SC)[20] [Eq. (1)] and the neural transfer function (NTF).[20,21] The NTF was computed as the product of the EmG contrast sensitivity model and the oblique effect[22] [Eq. (2)]. This function was included in the computation of the PSF and the retinal images shown in the different figures by multiplying this function by the Fourier transform of the PSF in the Fourier domain and then returning to the image domain through the inverse Fourier transform

$$\text{Stiles-Crawford} = \exp\left[-\frac{0.10592}{2}(x^2 + y^2)\right], \quad (1)$$

$$\begin{aligned} \text{NTF} = &\left\{\exp\left(-\frac{f}{f_o}\right) - a \cdot \exp\left[-\left(\frac{f}{f_1}\right)^2\right]\right\} \cdot \\ &\cdot \left[\begin{array}{ll} \left(1 - \left\{1 - \exp\left[-\frac{(f-f_2)}{b}\right]\right\} \cdot \sin(2\theta)^2\right) & \text{if } (f > 3.48) \\ 1 & \text{if } (f <= 3.48) \end{array}\right], \end{aligned}$$
$$(2)$$

where $f_o = 33.36$ cycles/deg; $f_1 = 5.38$ cycles/deg; $f_2 = 3.48$ cycles/deg; $a = 0.92$; and $b = 13.57$ cycles/deg. The NTF must be normalized to one after computation. More information on the NTF and the values of the parameters can be found in Refs. 21 and 22.

We also included the neural contrast threshold (NCT) in the calculations.[23] This curve provides information on the minimum contrast that certain frequencies must have to be detected by the visual system. The intersection point between this curve and the real (OTF) allows for the determination of the cutoff frequency of the visual system. Values above the cutoff frequency were set to zero in the calculations.

The two VS criteria evaluated were VSOTF [Eq. (3)] and VS$_{\text{Combined}}$ [Eq. (4)] proposed by Thibos et al.[13] and Young et al.,[16] respectively

VSOTF
$$= \frac{\int_{-\infty}^{\infty}\int_{-\infty}^{\infty} \text{OTF}(f_x, f_y) \cdot \text{NTF}(f_x, f_y)\mathrm{d}f_x\,\mathrm{d}f_y}{\int_{-\infty}^{\infty}\int_{-\infty}^{\infty} \text{OTF}(f_x, f_y)_{\text{diffraction limited}} \cdot \text{NTF}(f_x, f_y)\mathrm{d}f_x\,\mathrm{d}f_y},$$
$$(3)$$

VS_{Combined}
$$= \frac{\int_{-\infty}^{\infty}\int_{-\infty}^{\infty} \text{MTF}(f_x, f_y) \cdot \left|1 - \frac{\text{PTF}(f_x, f_y)}{\pi}\right| \cdot \text{NTF}(f_x, f_y)\mathrm{d}f_x\,\mathrm{d}f_y}{\int_{-\infty}^{\infty}\int_{-\infty}^{\infty} \text{MTF}(f_x, f_y) \cdot \text{NTF}(f_x, f_y)\mathrm{d}f_x\,\mathrm{d}f_y}.$$
$$(4)$$

As mentioned in the introduction, while VSOTF provides information about the effect of contrast reduction due to aberrations, VS$_{\text{Combined}}$ weighs the effect of phase reversal and PTF modulation on final image quality (it is important to note that as we are studying nonsymmetrical phase masks we need to take not only contrast but also modulation of the PTF into account[16]).

To simulate the retinal image, we convolved the PSFs associated with the different object positions and the CPM with a line of four letter "E" with different orientations with size in logMar units of 0.1 (equivalent size in decimal units 0.8). In the case of the naked eye, we set the magnitude of the cubic component to zero ($A = 0$ μm and $B = 0$ μm).

3 Experimental Proof of Concept

Next, we developed an experimental proof of concept (see Fig. 1). For that purpose, we built an artificial eye consisting of a plano-convex lens with a focal length of 25.4 mm and a 1-in. diameter, a variable diaphragm, a 3× objective lens (with short focal length and a ratio of 3/1 between image and object distances), and an ORCA 285 Hamamatsu Photonics camera 8.1 micron pixel size (therefore effective pixel size 2.7 μm). A set of four different eye-charts scaled for the corresponding distances were placed at 6, 1, 0.6, and 0.4 m from the artificial eye to monitor different visual acuities (ranging between 0.22 and 0 in logMar units and 0.6 and 1 in decimal units). They were
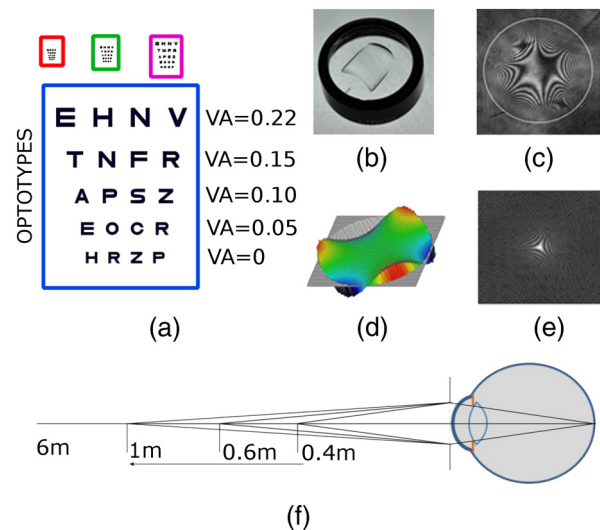

Fig. 1 Scheme of the experimental setup: (a) eye-chart in logMar units; (b) manufactured CPM; (c) interferogram of the CPM; (d) phase map of the CPM; (e) PSF of the CPM; and (f) eye-chart positions.
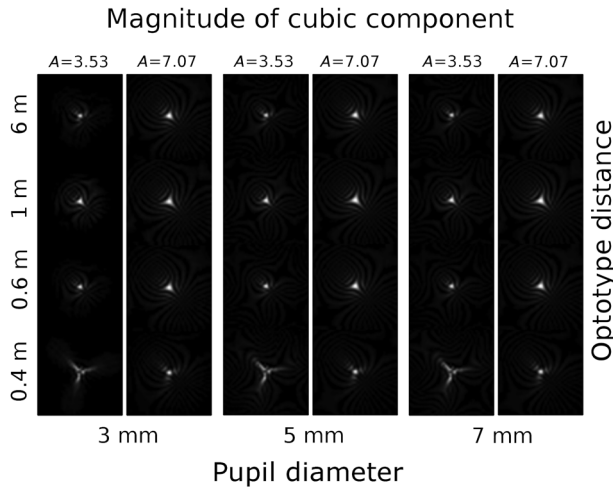
Magnitude of cubic component

Fig. 2 PSF images for CPM-3.53 and CPM-7.07 different pupil diameters and optotype positions.

printed on a transparency and back-lit with backscattered white light projected on a white panel to avoid reflection of the film. We should point out that initial trials on paper were unacceptable due to the blur of the letters caused by diffusion of the ink on the paper. We placed a CPM made using an ultraprecise micromilling technique on transparent polymethylmethacrylate directly in front of the artificial eye. The dimensions of the element were 10 mm × 10 mm with maximum sag of 1.8 mm. The optical quality of the plate was characterized with a point diffraction interferometer[24] presenting a trefoil magnitude of 4.80 μm @ 5-mm pupil diameter. Figure 1 shows the phase plate, the recorded interferogram, the resulting fitted phase, and the corresponding PSF. The iris was set to 3, 5, and 7 mm in diameter.

The measurement protocol was as follows: first of all, we make an image of an object placed at 1 m from the artificial eye to set B at 0.9 μm (this focus distance was maintained throughout the entire experiment). Second, we placed the corresponding eye charts at the different distances (starting at 0.4 m and then to
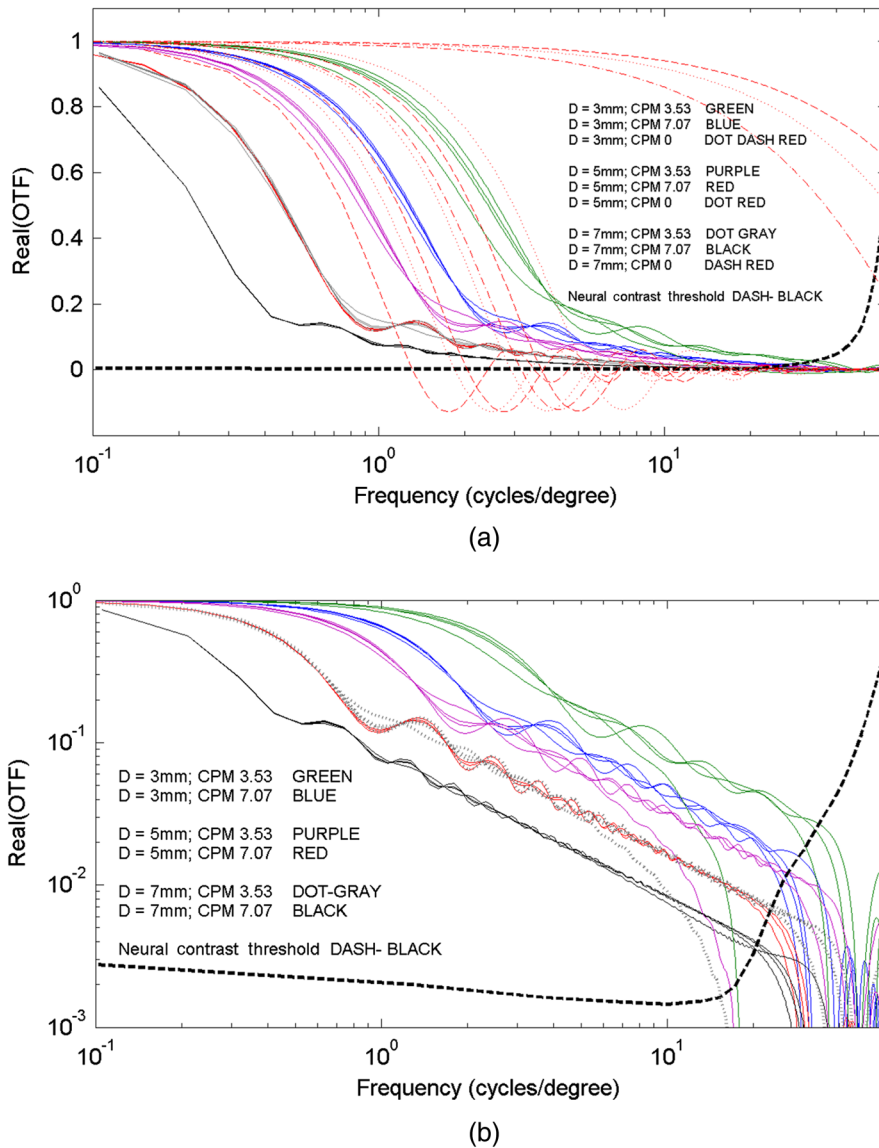

(a)

(b)

Fig. 3 (a) Semilog and (b) loglog representations of the real (OTF) for CPM-7.07, CPM-3.53, CPM-0, pupil diameters (3, 5, and 7 mm), for the four different optotype positions (6.0, 1.0, 0.6, and 0.4 m).

0.6, 1.0, and 6.0 m). For each distance, we took three images, with the three pupil sizes. This was repeated with and without the CPM. Lastly, the pictures were filtered with the NTF of Eq. (2) to mimic neuronally induced contrast improvement. For the case of the naked eye, we imaged with the artificial eye the chart of optotypes placed at 6 m.

4 Results of the Numerical Evaluation

To reduce the number of figures in this section, we only show those we believe are the most relevant for the analysis of the results. Figure 2 shows the simulated PSFs at the image planes of the different optotype distances (6.0, 1.0, 0.6, and 0.4 m) for different pupil sizes (3, 5, and 7 mm) and two different magnitudes of cubic component CPM-3.53 and CPM-7.07 generated with $A = 7.07$ μm and $A = 3.53$ μm, and $B = 0.9$ μm, respectively, and CPM-0 obtained with $A = 0$ μm and $B = 0$ μm.

Figure 3 compares the real part of the OTFs obtained for a presbyopic eye with CPM-3.53 and CPM-7.07, for the different optotype distances and for three different pupil diameters (7, 5, and 3 mm). The curves obtained with CPM-0 represent an emmetropic-presbyopic eye. The dashed, dotted, and dash-dotted curves correspond to the different real (OTF) obtained for the three pupil diameters and different optotype positions. In Fig. 3(a), we plot the real (OTF) on the semilogarithmic axis to show that without CPM some values are negative (phase inversion). In Fig. 3(b), we plot a loglog real (OTF) to show the intersection point between the real (OTF) and the NCT.

So far we have shown the behavior of PSF and real (OTF) of the phase element to compensate for presbyopia. Now, we will present simulations for retinal images. In Figs. 4–6, we show a set of retinal images obtained for the emmetropic–presbyopic eye and different pupil sizes and optotype positions and CPM. In Fig. 4, we present the case of CPM-0 (naked eye); in Fig. 5, CPM-3.53 and in Fig. 6, CPM-7.07. We should stress that the simulated images have not been postprocessed.

The retinal images presented in Figs. 5 and 6 provide a qualitative idea of the behavior of the phase element proposed to compensate for presbyopia in relation to changes in pupil diameter. Clearly, the CPM-7.07 with $A = 7.07$ μm provides better images in the sense of resemblance of the diffraction limited image for the whole range of pupil diameters and optotype
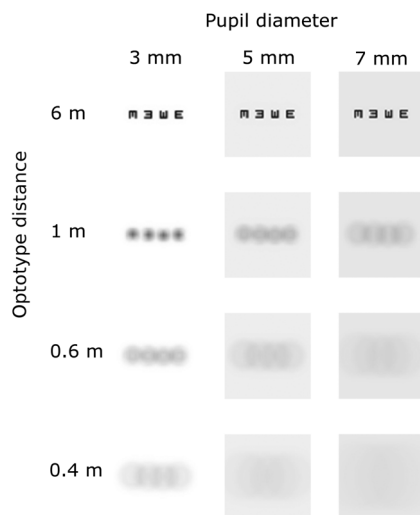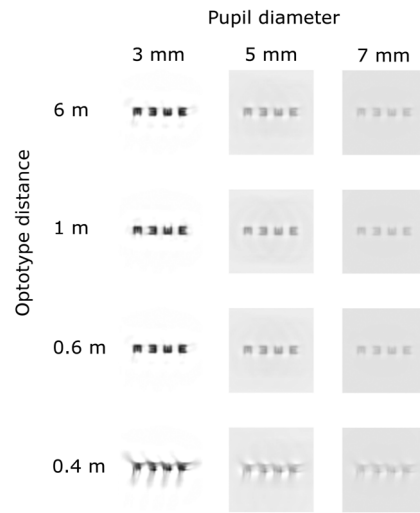

Fig. 5 Optotypes for CPM-3.53, pupil diameters (3, 5, and 7 mm) for the different optotype positions.

positions but at the expense of losing contrast. To obtain a quantitative estimate of the performance of the phase element, we computed the VS criteria (VSOTF[13] and VS$_{Combined}$[16]) and contrast measurements obtained with different criteria (RMS, Weber, and Michelson) and the correlation between the degraded image and the diffraction limited one. Table 1 shows grouped values of the metrics obtained for the different combinations of parameters.

Lastly, we present the experimental proof of concept of the dependence of the CPM solution on pupil diameter. Figure 7 shows the retinal images of the optotype chart placed at the different distances (6, 1, 0.6, and 0.4 m) and the three pupil diameters (3, 5, and 7 mm) obtained with the artificial eye. Notice that the experimental images have also been filtered with the NTF. In addition, the experiment was developed using white light, so chromatic aberration was present.

At this point, the reader might have the impression that the design of the CPM with the capricious combination of two Zernike polynomials is essential for the its correct performance. And that some sort of object spatial frequency promotion is
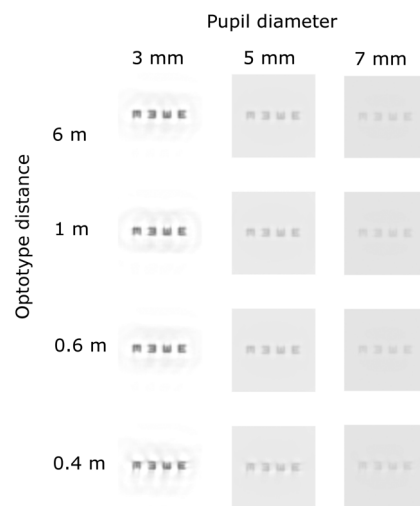

Fig. 4 Optotypes for CPM-0, pupil diameters (3, 5, and 7 mm) for the different optotype positions.

Fig. 6 Optotypes for CPM-7.07, pupil diameters (3, 5, and 7 mm) for the different optotype positions.

Table 1 Comparison of different metrics.

| Pupil diameter (mm)	CONTRAST RMS				CONT. WEBBER				CONT. MICHELSON				VSOTF				CORRELATION				VS$_{Combined}$			
	Optotype distance (m)																							
	6	1	0.6	0.4	6	1	0.6	0.4	6	1	0.6	0.4	6	1	0.6	0.4	6	1	0.6	0.4	6	1	0.6	0.4
Without CPM (CPM-0): A = 0; B = 0																								
3	0.38	1.00	0.49	0.11	0.31	0.88	0.33	0.04	0.19	0.78	0.20	0.02	0.07	1.00	0.10	0.03	0.71	1.00	0.70	0.34	0.71	1.00	0.72	0.48
5	0.12	1.00	0.20	0.06	0.04	0.92	0.10	0.02	0.02	0.85	0.05	0.01	0.03	1.00	0.04	0.01	0.40	0.99	0.56	0.09	0.53	1.00	0.56	0.53
7	0.07	1.00	0.09	0.04	0.03	0.95	0.04	0.01	0.02	0.90	0.02	0.00	0.01	1.00	0.02	0.01	0.10	0.99	0.12	0.12	0.52	1.00	0.53	0.52
CPM-3.53: A = 3.53 mm; B = 0.9 mm; @ 5 mm pupil																								
3	0.90	0.79	0.88	0.93	0.70	0.63	0.69	0.62	0.54	0.46	0.53	0.45	0.07	0.07	0.07	0.07	0.89	0.91	0.91	0.61	0.86	0.82	0.87	0.58
5	0.26	0.27	0.26	0.26	0.23	0.24	0.23	0.19	0.13	0.13	0.13	0.11	0.02	0.02	0.02	0.02	0.86	0.86	0.87	0.58	0.86	0.83	0.87	0.58
7	0.12	0.12	0.12	0.12	0.11	0.12	0.12	0.09	0.06	0.06	0.06	0.05	0.01	0.01	0.01	0.01	0.84	0.85	0.86	0.55	0.86	0.83	0.87	0.58
CPM-7.07: A = 7.07 μm; B = 0.9 mm; @ 5-mm pupil																								
3	0.41	0.40	0.41	0.41	0.33	0.32	0.33	0.33	0.20	0.19	0.20	0.20	0.04	0.04	0.04	0.04	0.89	0.87	0.89	0.86	0.81	0.78	0.80	0.80
5	0.13	0.13	0.13	0.13	0.12	0.11	0.12	0.11	0.06	0.06	0.06	0.06	0.01	0.01	0.01	0.01	0.86	0.83	0.85	0.83	0.81	0.78	0.80	0.80
7	0.06	0.06	0.06	0.06	0.06	0.06	0.06	0.06	0.03	0.03	0.03	0.03	0.00	0.00	0.00	0.00	0.84	0.82	0.83	0.82	0.81	0.78	0.81	0.80
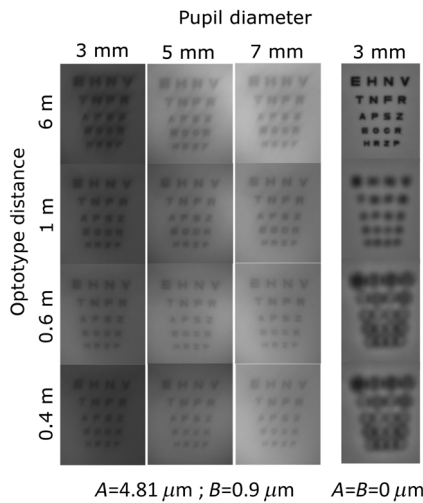
Pupil diameter

Fig. 7 NTF filtered retinal images obtained experimentally with the presbyopic artificial eye for the different optotype positions: with CPM $A = 4.81$ μm, $B = 0.9$ μm, and pupil diameters (3, 5, and 7 mm), and for the naked presbyopic eye with a 3-mm pupil diameter.
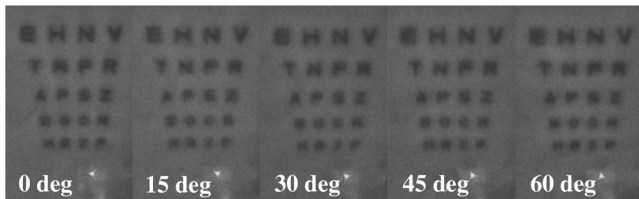

Fig. 8 NTF filtered retinal images and PSF of the system (eye + CPM) obtained experimentally with the presbyopic artificial eye with the optotype placed at 6 m, pupil diameter of 5 mm, and five different orientations of the CPM [angle of rotation with respect to initial position (0 deg, 15 deg, 30 deg, 45 deg, and 60 deg)].

obtained with the proposed CPM orientation that makes the images look nice, but that in any other orientation the images will be unacceptable. To clarify this, we show in Fig. 8(a) five images obtained with different rotations of the CPM. The rotation angles are (0 deg, 15 deg, 30 deg, 45 deg, and 60 deg) with respect to initial position. The images include in the bottom-right of the PSF of the eye with the CPM. So, we have registered simultaneously the image of the optotype and the PSF of the system. We can observe that although the PSF rotates when rotating the CPM the visual aspect of the optotype image keeps nearly constant. So, dependence of the performance of the CPM with its orientation seems to be low, although further analysis must be conducted in future works.

5 Discussion

In this paper, we studied the performance of the CPM in compensating for presbyopia in relation to changes in pupil diameter. Data presented suggest that CPM designs are very stable with only negligible changes in PSF, letter visibility, and VS criteria. It is worth noting that this solution remains stable for pupil diameter changes for all the optotype positions analyzed within the numerical and experimental validation.

Comparison of the performance of the CPM solutions in terms of the magnitude of the cubic component suggests that

while $A = 3.53$ μm provides higher image contrast, the range of clear vision is limited with poor results for close-up vision. In contrast, the CPM obtained with $A = 7.07$ μm provides a range of clear vision for near (0.4 m) and far vision (6 m) with smaller but enough image contrast for letter visibility.

The values of the real (OTF) obtained for the CPM solution for the different pupil diameters presented in Fig. 3 are well below the values of the defocused OTFs for low frequencies. However at middle frequencies, i.e., 5 to 30 cycles/deg, they do not cross to negative values thus avoiding loss of frequencies and contrast inversion as is the case in the real (OTF) with no cubic component. Moreover, although contrast is less than ideal, it is over the NCT thus providing enough contrast to read the letters.[25–28]

It is difficult to establish a clear criterion to assess the performance of extended depth of field solutions. VSOTF provides information mainly about the contrast transfer of the evaluated element, whereas $VS_{Combined}$ provides information on the amount of phase difference between the different frequencies transmitted by the system. Our results and those of other others show that it is important to quantify not only contrast loss but also PTF when evaluating nonsymmetrical phase elements.

Experimental results confirm numerical results. A nonoptimized CPM has broadened the range of clear vision from far to near and stabilized letter identification with respect to changes in pupil diameter. In addition, we notice that although chromatic aberration is present in the experimental validation, the blurring of the images due to this aberration has been masked by the codification of the PSF induced by the CPM.

We think that the results presented in this work show the potentiality of the CPM for being a solution to presbyopia.
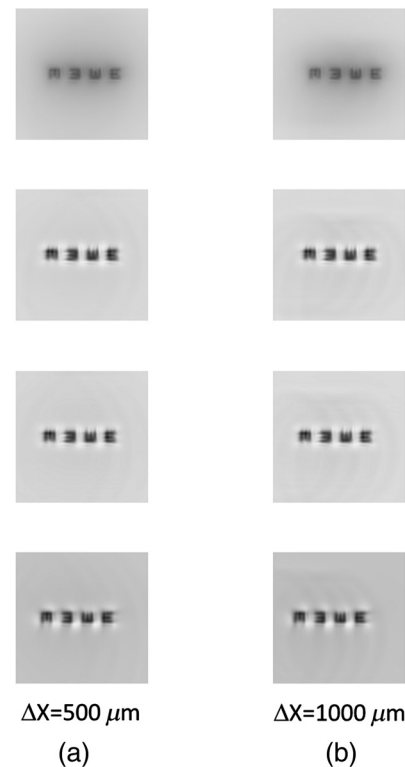

Fig. 9 Optotypes simulated for CPM-7.07, pupil diameters 5 mm and horizontal displacement of the CPM of (a) $\Delta X = 500$ μm and (b) $\Delta X = 1000$ μm.

However, additional studies concerning the influence or tolerance of the CPM solution to rotation and lateral displacement should be done (Fig. 8 presents a soft analysis of the tolerance to rotation, and numerical simulations made to test tolerance to lateral displacement show that it is close to $1000\mu m$). In addition, preliminary numerical and experimental studies related with the analysis of the coupling of the CPM with high-order aberrations present in the eye have shown the good tolerance to them, and the increase in the retinal image quality in comparison with the naked eye. However, deeper analysis has to be made to have a clear knowledge of the performance of the CPM solution in this case. In Fig. 9, as an example, we show the optotypes simulated considering a horizontal displacement of (a) $\Delta X = 500 \ \mu m$ and (b) $\Delta X = 1000 \ \mu m$. We can observe that the deformation of the images is not very pronounced with this lateral displacement, which is in the order of the one experienced, for example, by soft or rigid contact lenses.

Lastly, this potentiality has to be demonstrated by the validation of this kind of solutions on human subjects by assessing their visual experience and satisfaction. Having an equipment capable of generating different phase profiles based on adaptive optics technology would be of interest to have the flexibility demanded by this kind of experiment, where different designs must be tested with the same cohort of subjects.

6 Conclusions

We have shown that phase elements of the type 7.07 μm $(Z_3^3 - Z_3^{-3}) - 0.9 \ \mu m \ Z_2^0$ can compensate for presbyopia providing a broad enough range of clear vision to satisfy demands for clear vision at far and near working distances over a wide range of pupil diameters covering the full range found in the general population (3 to 7 mm). Nonsymmetrical phase elements should not be evaluated only in terms of contrast but should also include changes in PTF. Combination of VSOTF and VS$_{Combined}$ enables evaluation of contrast transfer and changes in PTF. Visualization of the retinal images made possible by the proposed phase elements continues to be important in evaluating their performance. The similarity between images obtained numerically and experimentally boosts confidence in the results.

Disclosures

Acknowledgments

References

1. A Glasser and M. C.W. Campbell, "Presbyopia and the optical changes in the human crystalline lens with age," *Vision Res.* **38**(2), 209–229 (1998).
2. W. N. Charman, "Developments in the correction of presbyopia I: spectacle and contact lenses," *Ophthalmic Physiol. Opt.* **34**, 8–29 (2014).
3. W. N. Charman, "Developments in the correction of presbyopia II: surgical approaches," *Ophthalmic Physiol. Opt.* **34**, 397–426 (2014).
4. E. S. Bennett, J. M. Jurkus, and C. A. Schwartz, *Clinical Manual of Contact Lenses*, 2nd ed., pp. 410–449, Lippincott Williams & Wilkins, Philadelphia (2000).
5. A. N. Simonov, G. Vdovin, and M. Rombach, "Cubic optical elements for an accommodative intraocular lens," *Opt. Exp.* **14**(17), 7757–7775 (2006).
6. J. Ares et al., "Presbyopia compensation with a quartic axicon," *Opt. Vis. Sci.* **82**(12), 1071–1078 (2005).
7. W.T. Cathey, Jr., "Extended depth of field optics for human vision," U.S. Patent 7025454B2 (2006).
8. Z. Zalevsky et al., "Thin spectacles for myopia, presbyopia and astigmatism insensitive vision," *Opt. Express* **15**, 10790–10803 (2007).
9. A. A. Gallego et al., "Visual Strehl performance of IOL designs with extended depth of focus," *Optom. Vision Sci.* **89**(12), 1702–1707 (2012).
10. K. Petelczyc et al., "Contrast transfer characteristics of the light sword optical element designed for presbyopia compensations," *J. Eur. Opt. Soc. Rapid Publ.* **6**, 11053 (2011).
11. J. Arines, C. Almaguer, and E. Acosta, "Potential use of cubic phase masks for extending the range of clear vision in presbyopes: initial calculation and simulation studies," *Ophthalmic Physiol. Opt.* **37**(2), 141–150 (2017).
12. J. D. Marsack, L. Thibos, and R. Applegate, "Metrics of optical quality derived from wave aberrations predict visual performance," *J. Vision* **4**, 322–328 (2004).
13. L. N. Thibos et al., "Accuracy and precision of objective refraction from wavefront aberrations," *J. Vision* **4**, 329–351 (2004).
14. R. Iskander, "Computational aspects of the visual Strehl ratio," *Optometry Vision Sci.* **83**(1), 57–59 (2006).
15. A. B. Watson and A. J. Ahumada, "Predicting visual acuity from wavefront aberrations," *J. Vision* **8**(4), 17 (2008).
16. L. K. Young, G. D. Love, and H. E. Smithson, "Accounting for the phase, spatial frequency and orientation demands of the task improves metrics based on the visual Strehl ratio," *Vision Res.* **90**, 57–67 (2013).
17. L. K. Young, G. D. Love, and H. E. Smithson, "Different aberrations raise contrast thresholds for single-letter identification in line with their effect on cross-correlation based confusability," *J. Vision* **13**(7), 12–12 (2013).
18. S. Ravikumar, A. Bradley, and L. Thibos, "Phase changes induced by optical aberrations degrade letter and face acuity," *J. Vision* **10**(14), 18–18 (2010).
19. L. N. Thibos et al., "Standards for reporting the optical aberrations of eyes," in *Vision Science and Its Applications*, Trends in Optics and Photonics Series, V. Lakshminarayanan, Ed., Vol. **35**, pp. 232–244, Optical Society of America, Washington, DC (2000).
20. R. Applegate, "Glenn fry award lecture 2002: wavefront sensing, ideal corrections, and visual performance," *Optometry Vision Sci.* **81**(3), 167–177 (2004).
21. A. B. Watson and A. J. Ahumada, "A standard model for foveal detection of spatial contrast," *J. Vision* **5**, 717–740 (2005).
22. A. B. Watson and A. J. Ahumada, "Modeling acuity for optotypes varying in complexity," *J. Vision* **12**(10), 19–19 (2012).
23. S. Bonaque-González et al., "Influence on visual quality of intraoperative orientation of asymmetric intraocular lenses," *J. Refractive Surg.* **31**(10) 651–657 (2015).
24. E. Acosta, R. Blendowske, and S. Chamadoira, "Modified point diffraction interferometer for inspection and evaluation of ophthalmic components," *J. Opt. Soc. Am. A* **23**, 632–637 (2006).
25. J. J. Mc Anany et al., "Object frequency characteristics of visual acuity," *Invest. Ophthalmol. Visual Sci.* **52**(13), 9534–9538 (2011).
26. A. P. Ginsburg, "Contrast sensitivity and functional vision," *Int. Ophthalmol. Clin.* **43**(2), 5–15 (2003).
27. H. Akutsu, H. E. Bedell, and S. S. Patel, "Recognition thresholds for letters with simulated dioptric blur," *Optometry Vision Sci.* **77**(10), 524–530 (2000).
28. F. Thor and F. Schwartz, "Effects of dioptric blur on Snellen and grating acuity," *Optometry Vision Sci.* **67**(1), 3–7 (1990).

Citlalli Almaguer is a PhD student at the Department of Applied Physics at the faculty of Óptica y Optometría of the University of

Santiago de Compostela. She received her degree in physics from the University of Guadalajara, Mexico, in 2010 and her MS degree in photonics and laser technology from the University of Vigo, Spain. Her areas of interest include wavefront coding, presbyopia correcting, and visual optics.

Eva Acosta is a professor at the faculty of physics of the University of Santiago de Compostela. His current research involves wavefront coding, plenotic, point diffractive interferometry, presbyopia, wavefront sensing, and visual optics.

Justo Arines received his BS, MS, and PhD degrees in physics and his MS degree in optics and optometry in 1997, 1999, 2006, and 2003, respectively, from the University of Santiago de Compostela, Spain. His current research involves wavefront coding, presbyopia, wavefront sensing, and visual optics.